

# Scaled-Particle Theory and the Length-scales Involved in Hydrophobic Hydration of Aqueous Biomolecular Assemblies

Henry S. Ashbaugh and Lawrence R. Pratt

*Theoretical Division, Los Alamos National Laboratory, Los Alamos, NM 87545, USA*

(Dated: October 30, 2018)

Hydrophobic hydration plays a crucial role in self-assembly processes over multiple length-scales, from the microscopic origins of inert gas solubility in water, to the mesoscopic organization of proteins and surfactant structures, to macroscopic phase separation. Many theoretical studies focus on the molecularly detailed interactions between oil and water, but the extrapolation of molecular-scale models to larger length-scale hydration phenomena is sometimes not warranted. Scaled-particle theories are based upon an interpolative view of that microscopic→macroscopic issue. We revisit the scaled-particle theory proposed thirty years ago by Stillinger (*J. Soln. Chem.* **2**, 141-158 (1973)), adopt a practical generalization, and consider the implications for hydrophobic hydration in light of our current understanding. The generalization is based upon identifying a molecular length, implicit in previous applications of scaled-particle models, that provides an effective radius for joining microscopic and macroscopic descriptions. We demonstrate that the generalized theory correctly reproduces many of the anomalous thermodynamic properties of hydrophobic hydration for molecularly sized solutes, including solubility minima and entropy convergence, successfully interpolates between the microscopic and macroscopic extremes, and provides new insights into the underlying molecular mechanisms. The model considered here serves as a reference for theories that bridge microscopic and macroscopic hydrophobic effects. The results are discussed in terms of length-scales associated with component phenomena; in particular we first discuss the micro-macroscopic joining radius identified by the theory, then we discuss in turn the Tolman length that leads to an analogous length describing curvature corrections of a surface area model of hydrophobic hydration free energies, and the length-scales on which *entropy convergence* of hydration free energies are expected.

## Contents

<b>I. Introduction</b>	1
A. An empirical length characteristic of a liquid in coexistence with a thin vapor	1
B. Sketch of experimental characteristics of hydrophobic hydration	2
<b>II. A primer on scaled-particle theory</b>	4
A. Classic scaled-particle theory	4
B. Revised scaled-particle theory	6
C. Computational implementation	7
<b>III. Application to hydrophobic hydration</b>	7
A. Cavity contact functions: the micro-macro joining boundary	7
B. Physical relevance of hard-core model solutes to structural theories of hydrophobic effects	8
C. Hydration thermodynamics of hydrophobic species: temperature signatures and solubility minima	9
D. Surface area dependence of hydration thermodynamic properties: curvature corrections and a Tolman length	10
E. Entropy convergence and solute size	11
<b>IV. Summary and conclusions</b>	13
<b>Acknowledgements</b>	14
<b>References</b>	14
<b>Figures</b>	16

## I. INTRODUCTION

The adage “oil and water don’t mix” dominates thinking about hydrophobic effects that are upheld, nearly universally, as the primary thermodynamic impetus for a number of important aqueous solution phenomena, including the environmental fate of pollutants, surfactant assembly, biological membrane formation, and the folding of globular proteins (Blokzijl and Engberts, 1993; Kauzmann, 1959; Simonson, 2003; Tanford, 1980). Enigmatic temperature signatures — such as the fact that many soluble proteins unfold both upon heating *and* cooling — offer the primary puzzles of hydrophobic effects, and are characteristic of the aqueous milieu. The ability to reproduce these temperature signatures from basic principles is essential for understanding the temperature range of binodal behavior of biophysical structures, and of aqueous phase nanotechnology designed by analogy with the molecular machinery of biophysics. Important aspects of these puzzles are that the hydrophobic temperature signatures are strongly affected by the spatial length-scales of the hydrophobic solution structures. This review focuses on recent progress in unraveling the puzzles of temperature signatures and length-scales characteristic of hydrophobic hydration.

### A. An empirical length characteristic of a liquid in coexistence with a dilute vapor

The calling-out of a particular length-scale, and the role it plays in statistical theories of solutions, has been a primary feature of recent discussions of hydrophobic effects (Lee, 1985; Lum *et al.*, 1999), though the length-scales noted in those two cases were different from each other. It is interesting, therefore, to consider length-scale issues more broadly. We can start by noting the classic suggestion of (Egelstaff and Widom, 1970) for a length-scale characteristic of a liquid in coexistence with a dilute vapor phase, namely the product of the liquid-vapor interfacial tension,  $\gamma$ , and the isothermal compressibility of the liquid,  $\kappa_T \equiv -\frac{1}{V} \left( \frac{\partial V}{\partial p} \right)_T$ ; see Fig. 1. The argument supporting this suggestion was physical, heuristic, and our discussion below of the scaled-particle theories will shed some additional light on this length-scale. It was immediately observed, however, that away from a critical region  $\gamma\kappa_T$  exhibited limited variation from liquid to liquid though the individual factors could differ by more than two orders of magnitude.

Fig. 1 shows that the temperature dependence of the length  $\gamma\kappa_T$  is qualitatively different for liquid water than it is for the organic solvents shown. This qualitatively different behavior is mostly ascribable to the fact that the compressibility of liquid water displays a minimum at 46°C; it decreases with increasing temperature for temperatures lower than this, and has a smaller net variation over this temperature domain compared to the other solvents. Though liquid water is much less compressible than are the other liquids, the liquid-vapor surface tension is much higher for water than for the other cases. This exemplifies the point that the product  $\gamma\kappa_T$  has smaller variations than do the individual factors. Still, liquid water is distinguished from liquids generically by peculiar temperature dependences. Similarly, the peculiarities of hydrophobic effects are temperature dependences that imply entropic stabilization of conformations and assemblies of hydrophobic solutes in aqueous solutions.

The theoretical description of hydrophobic effects has recently progressed markedly, and understanding the entropic interactions stabilizing of micelles, membranes, soluble proteins, and hierarchical biomolecular aggregation in aqueous solution has similarly advanced. It is now recognized that scaled-particle theories can properly describe primitive hydrophobic effects associated with the hydration of simple mono-atomic species. Scaled-particle theories identify — tentatively at first, but firmly as further information accumulates — a length separating microscopic from macroscopic descriptions of hydration structure. This establishes a radius at which microscopic and macroscopic descriptions of hydration structure can be effectively joined. Together with primitive constitutive information specific to liquid water, recognition of this joining radius provides an effective description of hydrophobic effects for meso-scale aqueous structures.

This paper traces those advances, specifically by laying out the basic view generalizing applications of scaled-particle approaches. We establish the micro-macroscopic joining length, discuss the length — analogous to the Tolman length — associated with curvature corrections of a surface area model of hydrophobic hydration free energies, and finally examine the length-scales on which *entropy convergence* of hydration free energies are expected.

### B. Sketch of experimental characteristics of hydrophobic hydration

Hydrophobic phenomena usually do not occur in isolation from other interaction effects. The solutes that motivate study of hydrophobic effects are typically molecularly complicated, water-soluble, amphiphilic chain molecules.

Researchers studying these systems have been comfortable, however, with a hydrophilic-hydrophobic dichotomy. It is common to identify contributions to the hydration free energy above and beyond obvious hydrophilic interactions as hydrophobic effects (Pratt, 1998). This is particularly true if the temperature dependences of the complementary hydrophobic interactions are also distinctive (Spolar *et al.*, 1989; Spolar and Record, 1994). A helpful review of hydrophilic electrostatic interactions involved in protein molecular structure with an emphasis on the multiple length-scales involved appeared recently (Simonson, 2003). The present discussion emphasizes model solutes, inert excluded volume models, that permit study of hydrophobic effects exclusively. Gases that are sparingly soluble in water, and small hydrocarbon molecules, can be brought into correspondence with hardcore molecular models. These models permit precision in isolating the temperature signatures that are the target of studies of hydrophobic effects.

High precision calorimetric studies show that unfavorable entropy changes upon transferring nonpolar solutes into water dominate hydration free energies at room temperature, and are only partly compensated by favorable enthalpy changes. These measurements are incongruous with *regular solution* notions, which ascribe insolubility to unfavorable cohesive interactions of the solute with water compared to water with itself (Lazaridis, 2001). Of foremost importance, the entropies and enthalpies of hydrophobic hydration are strongly temperature dependent, following from the large positive heat capacity changes observed. Thus, at elevated temperatures the roles of entropy and enthalpy are reversed, with unfavorable enthalpies dominating hydration free energies, partly compensated by favorable entropies. The resulting solubilities of nonpolar gases are nonmonotonic, exhibiting a solubility minimum between  $T = 310$  K and 350 K. Analogously, proteins undergo hot *and* cold denaturation (Brandts, 1964; Franks and Hatley, 1991) as

noted above, while ionic and nonionic surfactants display a minimum in their critical micelle concentrations with respect to temperature (Chen *et al.*, 1998a,b), pointing to a common underlying mechanism with the solubility behavior of nonpolar species.

The experimental entropy changes for a range of hydrophobic solutes intersect at values close to zero near  $T = 385$  K (Baldwin, 1986; Lee, 1991; Makhatadze and Privalov, 1995; Muller, 1993; Murphy *et al.*, 1990; Privalov, 1979; Privalov and Gill, 1988). The coincidence of this entropy convergence temperature for hydrocarbons with comparable behavior in protein unfolding has been used as empirical justification for the hydrophobic core model for protein folding, and has influenced the interpretation of biomolecular assembly. But in the complex context of soluble protein molecules, a clear relevance of entropy convergence can be questioned (Robertson and Murphy, 1997).

It has been traditionally argued that these hydrophobic entropy effects stem from orientational constraints on water molecules in the hydration shell of nonpolar solutes, constraints that maintain the integrity of a hydrogen-bonding network forming cage-like structures or microscopic *icebergs* (Frank and Evans, 1945). Theoretical studies of the impact of local clathrate formation about krypton in water conclude that literal clathrate structures are far too unfavorable to play a role in hydration thermodynamics (Ashbaugh *et al.*, 2003). Experimental probes of the local structure of water proximal to purely nonpolar solutes are scarce, and hampered by the low solute-concentrations attainable. The structures that have been studied by neutron and X-ray scattering techniques suggest that while water surely adopts orientational preferences in the hydration shell of nonpolar moieties, the solute-induced structure is more disordered than in ice or clathrate hydrates (Bowron *et al.*, 1998a,b; Broadbent and Neilson, 1994; DeJong *et al.*, 1997; Filipponi *et al.*, 1997).

Molecular-level investigations of hydrophobic hydration have been largely theoretical and simulation efforts (Henderson, 2002; Hummer *et al.*, 1998, 1996; Pierotti, 1976; Pohorille and Pratt, 1990; Pratt, 2002; Pratt and Pohorille, 1992; Stillinger, 1973). Water structure in the vicinity of hydrophobic species, including orientational preferences, has been connected to the entropies of hydrophobic hydration by a correlation function expansion (Ashbaugh and Paulaitis, 1996; Lazaridis and Paulaitis, 1992; Silverstein *et al.*, 2001). Pratt and Pohorille, on the other hand, demonstrated that the low solubility of atomic solutes in water arises from the narrow distribution of cavity-opening fluctuations in water (Pratt and Pohorille, 1992, 1993). With connections to the Pratt-Chandler theory (Pratt and Chandler, 1977) and its Gaussian field interpretation (Chandler, 1993; Lum *et al.*, 1999), an information theoretic (IT) model (Hummer *et al.*, 1998, 2000) then provided a quantitative link between the microscopic density fluctuations determined from water oxygen

pair correlations and the hydration free energies of hard solutes. More importantly, the IT model implicated the unusual equation-of-state properties of water as a dominant factor in hydrophobic hydration, differentiating water from other common solvents.

In addition to capturing temperature and pressure effects associated with hydrophobic hydration and interactions (Hummer *et al.*, 1998), the IT model provides a facile description of the enhanced solubility of nonpolar species in  $D_2O$  compared to  $H_2O$  as a result of differences in the isothermal compressibilities of these isotopic alternative forms of water (Hummer *et al.*, 2000).

The latter point suggests again the length  $\gamma\kappa_T$  of Fig. 1, because of the involvement of the measured isothermal compressibility with its specific temperature dependence. But the product  $\gamma\kappa_T$  involves the surface tension  $\gamma$  also, and the surface tension has been invoked in empirical correlations connecting measurable properties of liquid water and hydrophobic effects. Years ago, however, (Tanford, 1979) pointed out the large discrepancy between the measured water-hydrocarbon interfacial tension and the effective microscopic surface tensions obtained from hydrocarbon solubility data. A correspondence between macroscopic and microscopic surface tensions has been contentious because of their fundamentally different temperature dependence. As noted above, it is temperature dependences that have been the basic puzzles of hydrophobic effects.

More recent examples of the distinction between molecular and macroscopic hydrophobic interactions are found in measurements of the long-range attractive force between macroscopic hydrophobic surfaces (Christenson and Claesson, 1988; Israelachvili and Pashley, 1982; Pashley *et al.*, 1985) which have not been explained on the basis of molecular hydrophobic effects. Vibrational sum frequency spectroscopy suggests that hydrogen-bonding of water molecules is weaker at macroscopic water-carbon tetrachloride and water-hexane interfaces than near individual hydrophobic species dissolved in water (Scatena *et al.*, 2001). The lack of a definitive interpretation of these surface force measurements, and the changes in water energetics at macroscopic interfaces underscores the need for a quantitative theory beyond molecular hydrophobic effects. In general, the need for a unified, quantitative description of both molecular and macroscopic hydrophobic phenomena arises because hydrophobic driving forces play an important role in self-assembly on multiple length-scales and the fact that quantitative descriptions of these driving forces are derived from molecular solubility data, macroscopic interfacial tension measurements, or interpolations of these quantities (Ashbaugh *et al.*, 1999; Ashbaugh and Paulaitis, 2001; Gallicchio *et al.*, 2000; Hermann, 1977; Sharp *et al.*, 1991; Tanford, 1979).

(Lum *et al.*, 1999) suggested bridging these disparate length-scales by incorporating a Gaussian field theory for molecular level fluctuations with mean-field theory for

larger scale structures ultimately responsible for macroscopic phase transitions. Their approach successfully predicts many of the thermodynamic anomalies characteristic of small molecule hydration, and goes further, predicting the onset of long-range hydrophobic forces between surfaces as a result of an aqueous liquid-vapor phase transition in confined geometries. Indeed surface force apparatus studies of the long-range hydrophobic interaction (Christenson and Claesson, 1988) and simulations of water confined between repulsive oblate ellipsoids observed cavitation between nonpolar surfaces (Huang *et al.*, 2003), consistent with theoretical predictions. Mean-field modeling and simulations of methane clusters, however, suggest that when ubiquitous attractive interactions between water and hydrophobic surfaces are taken into account, surface and confinement induced local structural changes are suppressed (Ashbaugh and Paulaitis, 2001; Ashbaugh *et al.*, 2004; Chau, 2003; Dzubiella and Hansen, 2003; Truskett *et al.*, 2001). Moreover, experiments on the effects of electrolyte addition and degassing on the range of surface forces, and the stability of surfactant free aqueous emulsions challenge the theoretical predictions (Considine *et al.*, 1999; Kokkoli and Zukoski, 1998; Pashley, 2003; Pashley *et al.*, 2004).

A conceptual basis for unifying molecular and macroscopic hydrophobic hydration can be found in scaled-particle theory (SPT). Thirty years ago (Stillinger, 1973) presented an influential paper on the application of the classic SPT of Reiss (Pierotti, 1976; Reiss, 1965, 1977; Reiss *et al.*, 1959) to the hydration thermodynamics of purely excluded volume solutes. The purpose of that paper was, in part, to illuminate the pitfalls and difficulties in applying classic SPT, originally developed for hard-sphere fluids, to aqueous solvents (Ben-Naim and Friedman, 1967). In doing so Stillinger opened up new avenues of inquiry into hydrophobic hydration within the context of SPT. Nevertheless, direct exploration of the validity and consequences of Stillinger’s revised theory have been rare (Pratt and Pohorille, 1992, 1993). We presently revisit SPT and critically discuss its implications in light of our current understanding of hydrophobic hydration. For the first time, we demonstrate that the revised SPT reproduces many of the characteristic thermodynamic signatures of molecular hydrophobic effects and can be used to extend the results of molecular simulations of small hard hydrophobic solutes in water to meso- and macroscopic surface hydration. The present analysis provides insights into the differences and similarities for hydrating molecular and macroscopic surfaces. In addition, we examine the validity of surface area correlations commonly used in biophysical models for hydration thermodynamics over a range of length-scales, as well as the origins of entropy convergence behavior at molecular lengths scales and how solute size moderates the convergence temperature.

## II. A PRIMER ON SCALED-PARTICLE THEORY

### A. Classic scaled-particle theory

The chemical potential of a hydrated mono-atomic solute, ‘A’, can be expressed formally as

$$\mu_A(\text{aq}) = kT \ln [\rho_A(\text{aq}) \Lambda_A^3] + \mu_A^{\text{ex}}(\text{aq}) \quad (1)$$

where we have adopted Ben-Naim’s standard state in the definition of the chemical potential (Ben-Naim and Marcus, 1984). Here  $k$  is Boltzmann’s constant,  $T$  is the temperature,  $\rho_A(\text{aq})$  is the solute number density in the solution,  $\Lambda_A$  is the thermal de Broglie wavelength of the solute, and  $\mu_A^{\text{ex}}$  is the excess chemical potential, *i.e.*, the coupling work of turning on interactions between the solute and water, which disappears if those interactions vanish. At thermal equilibrium the Ostwald partition coefficient determining the distribution of the solute between an aqueous and ideal gas [ $\mu_A^{\text{ex}}(\text{ideal}) = 0$ ] phase at infinite dilution is (Pollack, 1991)

$$K_{\text{eq}} = \frac{\rho_A(\text{aq})}{\rho_A(\text{ideal})} = \exp[-\mu_A^{\text{ex}}(\text{aq})/kT]. \quad (2)$$

Thus, the excess chemical potential is central to resolving the aqueous solubility of the solute. Confining our discussion to impenetrable hard sphere (HS) solutes, the solute excess chemical potential in water is

$$\mu_A^{\text{ex}}(\text{aq}) = -kT \ln p_0(R) \quad (3)$$

where the insertion probability,  $p_0(R)$ , is the probability that a solute-sized stencil randomly placed in water is devoid of water oxygen centers; this follows directly from Widom’s potential distribution theorem for species interacting with a hard potential (Pratt *et al.*, 1999; Widom, 1982). The solvent accessible radius,  $R$ , is the radius of closest approach between the solute center and a water oxygen. The solvent accessible radius is the sum of the van der Waals radius of a water molecule and the radius of the hard-sphere solute, *i.e.*,  $R = (\sigma_{\text{WW}} + \sigma_{\text{AA}})/2$ . The insertion probability is the fractional free volume offered by the solution — or the *available* volume in a more specialized language attributed to Boltzmann (Stell, 1985), *i.e.*,  $p_0(R) = V_{\text{free}}/V_{\text{total}}$ .

Figure 2 gives a physical picture of this available volume. Given a molecular snapshot of liquid water — the left box in Fig. 2 —  $V_{\text{free}}$  is determined by the points at which a hard sphere could be successfully implanted. Graphic display of those successful placements thus yields a negative image — the right box in Fig. 2 — of the molecular configuration from which the analysis started.  $V_{\text{free}}$  decreases with increasing cavity radius, as successful insertions become increasingly rare.  $p_0(R)$  is subsequently determined as an ensemble average over a large number of molecular configurations.

An alternative relationship for the chemical potential that draws a connection to the structure of water in the

vicinity of the solute is

$$\mu_A^{\text{ex}}(\text{aq}) = kT \int_0^R \rho_W G(r) 4\pi r^2 dr \quad (4)$$

where  $\rho_W G(r)$  is the density of water in contact with a hard solute of contact radius  $r$  (Stillinger, 1973). The product  $kT\rho_W G(r)$  has units of force/area, and is the pressure due to solvent collisions with the hard surface of the solute. The chemical potential then is the reversible pressure-volume work required to expand the solute into the solution. The etymology of scaled-particle theory derives from this expression (Reiss, 1965, 1977) since the solute is introduced by scaling-up from a particle with a solvent accessible radius of zero to a final size of  $R$ . The relationship between the contact function and the insertion probability is

$$G(R) = -\frac{1}{4\pi R^2 \rho_W} \frac{\partial \ln p_0(R)}{\partial R}, \quad (5)$$

as determined by differentiation of Eq. (4). For sufficiently small solute cavities that only one solvent molecule might fit within the cavity boundary, the insertion probability is

$$p_0(R \rightarrow 0) = 1 - \frac{4\pi}{3} \rho_W R^3. \quad (6)$$

This is merely  $V_{\text{free}}/V_{\text{total}}$  in the case that the solute is so small that it never interacts with more than one solvent molecule exclusion sphere at once. Then the excluded volume is  $(4\pi R^3/3)N_W$ ; the more general case comes-up below. The expression corresponding to Eq. 6 for the contact function is

$$G(R \rightarrow 0) = \frac{1}{1 - \frac{4\pi}{3} \rho_W R^3}. \quad (7)$$

These expressions are accurate in solvents with realistic interactions for cavities up to a radius of  $R \approx \sigma_{\text{WW}}/2$ , and are exact in hard sphere fluids then because the solute corresponds to a point particle with a van der Waals radius of zero. Larger hard-sphere solutes can contact

more than one solvent molecule at once, and addressing larger solutes requires information on dauntingly complicated multi-body correlations.

In the limit of a macroscopically large cavity, the contact correlation function can be represented as an asymptotic expansion in  $1/R$

$$G(R) \sim \sum_{j \geq 0} \frac{G_j}{R^j}. \quad (8)$$

Retaining contributions up to  $j = 2$  yields an expression equivalent in form to that required by classical thermodynamics for the force acting on the cavity surface (Henderson, 2002; Pierotti, 1976; Reiss, 1965, 1977; Stillinger, 1973)

$$kT\rho_W G(R) \sim p + \frac{2\gamma_\infty}{R} - \frac{4\gamma_\infty\delta}{R^2} \quad (9)$$

where  $p$  is here to equal the liquid saturation pressure  $p_{\text{sat}}$ ,  $\gamma_\infty$  is henceforth the surface tension of a flat interface that was denoted by  $\gamma$  above, and  $\delta$  (Tolman, 1949) describes the initial curvature correction to the surface tension.<sup>a</sup> The coefficient  $G_3$  is zero so that the chemical potential is free of logarithmic contributions (Stillinger and Cotter, 1971) though analyses of the possibility of logarithmic corrections are still of interest (Evans *et al.*, 2004, 2003). Higher order terms in the asymptotic expansion are not generally available. Such considerations motivated (Reiss *et al.*, 1959) to truncate Eq. (8) after the initial curvature correction in order to develop a tractable, physically reasonable model for the contact function.

<sup>a</sup> The notation of Eq. (9) follows a typographic confusion widespread across the present problem.  $\delta$  here is one-half the conventional Tolman length. Expressed more basically the final term on Eq. (9) is  $(2\gamma_\infty/R)$  times the Tolman length. See (Henderson, 2002; Moody and Attard, 2001). We thank J. R. Henderson for a discussion of this point.

Evaluating the  $j = 0$  term in Eq. (8) with the measured equation of state, and the  $j = 1, 2$  terms in the expansion by requiring the microscopic and macroscopic limits smoothly meet at  $\sigma_{\text{WW}}/2$ , yields

$$G(R) = \begin{cases} \frac{1}{1 - \frac{4\pi}{3} \rho_W R^3}, & R \leq \sigma_{\text{WW}}/2 \\ \frac{p_{\text{sat}}}{kT\rho_W} + \left[ \frac{2+\eta}{(1-\eta)^2} - \frac{2p_{\text{sat}}}{kT\rho_W} \right] \left( \frac{\sigma_{\text{WW}}}{2R} \right) + \left[ -\frac{(1+2\eta)}{(1-\eta)^2} + \frac{p_{\text{sat}}}{kT\rho_W} \right] \left( \frac{\sigma_{\text{WW}}}{2R} \right)^2, & R > \sigma_{\text{WW}}/2 \end{cases} \quad (10)$$

where  $\eta = \frac{\pi}{6} \rho_W \sigma_{\text{WW}}^3$  is the solvent packing fraction. Integration of the contact function yields the excess chemical potential

$$\frac{\mu_A^{\text{ex}}}{kT} = \begin{cases} -\ln \left( 1 - \frac{4\pi}{3} \rho_W R^3 \right), & R \leq \sigma_{\text{WW}}/2 \\ \left[ -\ln(1-\eta) + \frac{9\eta^2}{2(1-\eta)^2} - \frac{\eta p_{\text{sat}}}{kT\rho_W} \right] + \left[ -\frac{3\eta(1+2\eta)}{(1-\eta)^2} + \frac{3\eta p_{\text{sat}}}{kT\rho_W} \right] \left( \frac{2R}{\sigma_{\text{WW}}} \right) + \left[ \frac{3\eta(2+\eta)}{2(1-\eta)^2} - \frac{3\eta p_{\text{sat}}}{kT\rho_W} \right] \left( \frac{2R}{\sigma_{\text{WW}}} \right)^2 + \frac{\eta p_{\text{sat}}}{kT\rho_W} \left( \frac{2R}{\sigma_{\text{WW}}} \right)^3, & R > \sigma_{\text{WW}}/2. \end{cases} \quad (11)$$

Eqs. (10) and (11) constitute the classic SPT originally developed for the hard sphere fluid (Reiss, 1965, 1977), but which was subsequently applied to water by (Pierotti, 1976) and (Lee, 1985). Fundamental difficulties arise in the application of classic SPT to water, however, including the erroneous prediction that the surface tension of water increases with temperature and passes through a maximum near  $T = 425$  K (Stillinger, 1973).

## B. Revised scaled-particle theory

The scaled-particle model described above incorporates little molecular detail beyond the assigned van der

Waals diameter,  $\sigma_{\text{WW}}$ , that might differentiate water from other solvents, and thereby limits the interpretation of complex hydration phenomena. To consider this problem more generally, we note that the insertion probability is formally expressed on the basis of solvent structure by an inclusion-exclusion development (Reiss, 1965, 1977; Stillinger, 1973)

$$p_0(R) = 1 + \sum_{n \geq 1} \frac{(-\rho_{\text{W}})^n}{n!} \int_{V(R)} \dots \int_{V(R)} g^{(n)}(\mathbf{r}_1 \dots \mathbf{r}_n) d^3 r_1 \dots d^3 r_n \quad (12)$$

where  $V(R) = 4\pi R^3/3$  is the observation volume, and  $g^{(n)}(\mathbf{r}_1 \dots \mathbf{r}_n)$  are the  $n$ -body solvent oxygen distribution functions. The terms in this series vanish for  $n$  exceeding the maximum number of solvent molecular centers that can be packed into a sphere of volume  $4\pi R^3/3$ . It is on this basis that the limiting result, Eq. (6), is established. As noted above, these distribution functions are complicated, not routinely available beyond the pair-distribution function ( $n = 2$ ), and there has been only one detailed investigation of terms beyond 2nd order (Gomez *et al.*, 1999; Pratt *et al.*, 1999). Considering the small cavity pair-correlation ( $n = 2$ ) contribution and the asymptotic macroscopic thermodynamic limits, Stillinger proposed a revised expression for the cavity contact function (Stillinger, 1973)

$$G(R) = \begin{cases} \frac{1 + \frac{\pi \rho_{\text{W}}}{R} \int_0^{2R} g^{(2)}(r) r^2 (r-2R) dr}{1 - \frac{4\pi}{3} \rho_{\text{W}} R^3 + \left(\frac{\pi \rho_{\text{W}}}{R}\right)^2 \int_0^{2R} g^{(2)}(r) (r^3/6 - 2R^2 r + 8R^3/3) dr}, & R \leq R^* \\ \frac{p_{\text{sat}}}{kT \rho_{\text{W}}} + \frac{2\gamma_{\infty}}{kT \rho_{\text{W}} R} - \frac{4\gamma_{\infty} \delta}{kT \rho_{\text{W}} R^2} + \frac{\lambda}{R^4}, & R > R^* \end{cases} \quad (13)$$

where  $R^*$  is the radius at which  $n = 3$  correlations begin to contribute to the cavity insertion probability of Eq. 12. While the experimental pressure, surface tension, density, and solvent radial distribution function are employed,  $\delta$  and  $\lambda$  are treated as adjustable parameters chosen so that the small cavity and macroscopic limits of the contact function join smoothly at  $R^*$ . This expression incorporates molecular information on the pair structure of water as well as the known macroscopic properties of bulk water and its interfacial behavior, and thereby is expected to discriminate more sensitively between water (Ashbaugh and Paulaitis, 2001) and other solvents (Huang and Chandler, 2000a). Indeed, it has been demonstrated by extensive molecular simulations that Eq. (13) provides a description superior to the classic SPT expression Eq. (10) of the solvent contact density for solutes several times larger than the solvent.

Stillinger's revised SPT prediction for  $G(R)$  relies on the assumption that multi-body water correlations at intermediate, but molecule-sized, solute radii are adequately represented by the parameters  $\delta$  and  $\lambda$  fitted at a radius  $R^*$ . Numerical experimentation (Pratt and Pohorille, 1992) with this parameterization

shows that the revised SPT is most sensitive to the parameter  $R^*$ . This parameterization might be improved by involving results over a range of radii, including solute sizes for which multi-body correlations are significant. While this information is not readily available experimentally, multi-body correlation contributions to the hard-sphere solute chemical potential can be interrogated by direct evaluation of the insertion probabilities from molecular simulations of water. In the spirit of Stillinger's revised SPT, we interpolate between the chemical potential evaluated for molecular length-scales from simulation, and the macroscopic thermodynamic limit

$$\mu_{\text{A}}^{\text{ex}}(R) = -kT \ln p_0(R)|_{\text{sim}} f(R) + \mu_{\text{A}}^{\text{ex}}(R)|_{\text{macro}} [1 - f(R)] \quad (14)$$

where  $f(R)$  is a switching function equal to one below  $R_{\text{sim}}$  and zero above  $R_{\text{macro}}$ , smoothly interpolating between these between these two limits. Presently we use a cubic spline interpolating function, though other reasonable functions yield essentially indistinguishable predictions. The macroscopic chemical potential, determined by integration of the macroscopic cavity expres-

sion Eq. (13) in

$$\mu_A^{\text{ex}}(R)|_{\text{macro}} = -\frac{4\pi kT\rho_W\lambda}{R} + \epsilon - 16\pi R\gamma_\infty\delta + 4\pi R^2\gamma_\infty + \frac{4\pi}{3}R^3\rho_{\text{sat}} \quad (15)$$

Rather than fitting the microscopic and macroscopic limits at a single point as in Eq. (13), the parameters  $\delta$ ,  $\lambda$ , and the integration constant  $\epsilon$  are fitted to the simulation results between  $R_{\text{sim}}$  and  $R_{\text{macro}}$ . The contact correlation function is then determined by differentiation of the chemical potential [Eq. (5)]. An additional benefit of fitting Eq. (15) to the simulation insertion probabilities is that we do not have to evaluate numerically first and second derivatives of the simulated insertion probabilities, which become more statistically uncertain with increasing cavity size.

### C. Computational implementation

The computational implementation follows standard procedures for sampling molecular configurations of liquid water, and builds from the original work of (Pohorille and Pratt, 1990; Pratt and Pohorille, 1992, 1993) in evaluating cavity statistics therefrom. Water configurations were generated using Monte Carlo simulations in the canonical ensemble (Frenkel and Smit, 2002). Bulk water was modeled using 268 SPC/E water molecules with periodic boundary conditions (Berendsen *et al.*, 1987). SPC/E was chosen because it provides an accurate representation of the structure, equation-of-state, and interfacial tension of liquid water over a broad range of temperatures (Alejandre *et al.*, 1995; Hura *et al.*, 2003). Lennard-Jones potential interactions were evaluated smoothly truncating the potential based on the separation of water oxygen atoms between 9.5 Å and 10 Å, while longer ranged electrostatic interactions were calculated using Ewald summation with conducting boundary conditions (Frenkel and Smit, 2002). Simulations were carried out from  $T = 260$  K to 470 K in 10 K increments at the experimental liquid density along the saturation curve and into the supercooled regime (Hare and Sorensen, 1986). After an equilibration phase of at least  $10^5$  MC passes (where one pass corresponds to one attempted move per water molecule with 30% move acceptance),  $5 \times 10^6$  MC production passes were carried out for analysis of thermodynamic averages. After each 50 MC passes,  $10^5$  particle insertions were attempted to estimate  $p_0(R)$ , so a total of  $10^{10}$  insertions were attempted at each temperature. Statistical uncertainties were determined by grouping results into block averages over  $10^6$  MC passes each.

## III. APPLICATION TO HYDROPHOBIC HYDRATION

### A. Cavity contact functions: the micro-macro joining boundary

The cavity contact function at  $T = 300$  K is shown in Fig. 3. Beginning at a value of one at zero radius, the cavity contact density increases with increasing  $R$ . Simulation values of  $G(R)$  appear to plateau at a maximum near 3 Å. Just beyond this radius, the simulation results for  $G(R)$  become progressively noisy as a result of poor sampling of infrequent large cavity fluctuations. Detailed calculations for specific values of  $R$  greater than 3 Å (Ashbaugh and Paulaitis, 2001) have established that this is indeed the region of a maximum in  $G(R)$ , and that  $G(R)$  is qualitatively described by Stillinger’s revised scale particle model. A dominating observation is that this curve imposes a non-arbitrary definition of a length-scale for the present problem: the radius  $R_{\text{max}}$  at which  $G(R)$  is a maximum. Solutes with smaller radii are identified as intrinsically microscopic in scale. The description of larger solutes can be built from a macroscopic perspective. An interpolative strategy extending to large solutes, such as that adopted here, is likely to be effective if the region at which the molecular and macroscopic expressions are joined encompasses  $R_{\text{max}}$ . The revised SPT fit, determined by differentiation of Eq. (14) fitted to the simulation insertion results between  $R_{\text{sim}} = 2.5$  Å and  $R_{\text{macro}} = 3.5$  Å, extends  $G(R)$  to  $R$  larger than observed directly. The revised SPT result places the maximum contact density at  $R = 3.0$  Å where  $G(R) \approx 2.3$ . Solutes of this size are candidates for *most hydrophobic* because the compressive pressure exerted by the solvent is largest in this case; see Fig. 4.

Beyond this maximum, water pulls away from the cavity surface with increasing size. At the size  $R \approx 10$  Å the contact density equals the bulk density of water, decreasing further for larger cavities. In the limit  $R \rightarrow \infty$ , the contact correlation approaches  $\frac{p_{\text{sat}}}{\rho_W kT} \approx 2 \times 10^{-5}$  for water at  $T = 300$  K, and the pressures here are sufficiently low that they do not influence the contact function for molecular and mesoscopic cavities at any of the temperatures considered.

This apparently anomalous drying behavior was anticipated by (Stillinger, 1973), and has only recently been confirmed by molecular simulations in Lennard-Jones and aqueous solvents (Ashbaugh and Paulaitis, 2001; Huang and Chandler, 2000a). The surface drying has been previously interpreted in terms of an effective expulsion potential between water and the solute cavity (Hummer and Garde, 1998; Weeks *et al.*, 1998). In bulk water, the individual water molecules feel attractive interactions with the other water molecules, and the average force on a water molecule in the bulk is zero. To approach a large solute, however, a water molecule must shed hydration partners and/or limit their possible configurations. This unbalances the interactions with the aqueous medium and gives rise to an additional repul-

sive force between a water molecule and the surface. If the solute is unable to compensate for these lost interactions to counter the cavity expulsion potential, water is repelled by the surface.

The classic SPT prediction for the contact function [Eq. (10)] is in qualitative agreement with the simulation and revised SPT results [Fig. 3]. Classic SPT predicts a maximum in the contact density, followed by a decrease to values below the bulk density of water with increasing cavity radius. The quantitative agreement is poor, however, even if the effective diameter,  $\sigma_{\text{WW}}$ , of water is treated as an adjustable parameter. Notably, classic SPT predicts that the maximum in  $G(R)$  is shifted to smaller radii of  $R \approx 2 \text{ \AA}$ . Water has an open structure favoring larger cavities at these packing fractions (Pohorille and Pratt, 1990; Pratt and Pohorille, 1992). The resulting maximum in the pressure acting on the solute surface,  $kT\rho_{\text{W}}G(R)$ , then is shifted out to larger cavity radii for water.

If the objective of classic SPT is to reproduce the chemical potentials of solutes using Eq. (11) up to radii of  $R \approx 3.3 \text{ \AA}$ , encompassing the sizes of a number of nonpolar gases, a typical diameter,  $\sigma_{\text{WW}}$ , of water fitted to experimental data is  $2.7 \text{ \AA}$  (Lee, 1985), though a more appropriate value based on the simulation results reported in Fig. 3 is  $2.8 \text{ \AA}$ . In this case, the fitted radius of water splits the difference between the over-prediction of  $G(R)$  at intermediate radii by the classic SPT, and the under-prediction of  $G(R)$  at radii close to the maximum solute size to balance out these inaccuracies in the calculation of the chemical potential. This  $\sigma_{\text{WW}}$  assigned to water molecules then is a consequence of the fitting, and does not contribute to the interpretation of the molecular signatures of hydrophobicity. Indeed, if we extend the predictions of classic SPT outside the range fitted for small solutes, we find the theory under-predicts the hydration free energies of mesoscopic cavities, and that a larger water diameter —  $\sigma_{\text{WW}} \approx 2.9 \text{ \AA}$ ! — is required to match the drying observed in  $G(R)$  [Fig. 3].

While the variation of this size parameter may seem small, the chemical potential depends on the integral of Eq. 4, and small differences in  $\sigma_{\text{WW}}$  significantly alter the predictions. Broadly viewed, this is the natural observation that slight adjustment of boundary information in boundary value problems can make large changes away from the boundary.

Revised SPT predictions for  $G(R)$  as a function of temperature are shown in Fig. 5. While all the curves are qualitatively similar, the magnitude of the contact function decreases with increasing temperature. Classic SPT fails to describe this temperature dependence of  $G(R)$ . Fig. 5 also indicates that the length defined by the maximum of this curve *decreases* with increasing temperature, consistent with the suggestion of Fig. 1. In following sections we use these revised SPT results to draw conclusions regarding the size and temperature dependence of the hydration of hydrophobic hard spheres.

The discussion in Sec. I.A of the length-scale  $\gamma_{\infty}\kappa_T$

sheds some light on the results of Fig. 5. Specifically, we can put together the crudest of models of the hydration free energies for the small-scale and large-scale problems, and in that way get a crude characterization of the length at which these different descriptions for  $G(\lambda)$  match. For the small-scale — but not the smallest-scale as in Eq. 6, the information theory approach suggested (Garde *et al.*, 1996; Pratt, 2002)  $\beta\mu_{\text{A}}^{\text{ex}} \approx \langle n \rangle_0^2 / 2 \langle \delta n^2 \rangle_0$ . If we evaluate everything on a macroscopic basis, then  $G(R) \approx \frac{\beta}{2\rho_{\text{W}}\kappa_T}$  from Eq. 5. This is an extremely crude estimate, but we rely only the trends with changes in temperature in the present argument. For the large-scale problem, we use  $\beta\mu_{\text{A}}^{\text{ex}} \approx 4\pi R^2\beta\gamma_{\infty}$ , expecting that the pressure will be negligibly low for this consideration. Then  $G(R) \approx \frac{\beta\gamma_{\infty}}{R\rho_{\text{W}}}$ . These two estimates match when  $R_{\text{max}} \approx 2\gamma_{\infty}\kappa_T$ . The first of these estimates, that from the information theory contribution evaluated on macroscopic information, is too large by about a factor of 4. Exploiting an empirical factor of 4 would bring the estimate  $R_{\text{max}} \approx 4 \times 2\gamma_{\infty}\kappa_T$  into a realistic range of molecular sizes. But the present argument is crude enough that only the dimensionally natural linear correlation with the length  $\gamma_{\infty}\kappa_T$  should be taken seriously.

## B. Physical relevance of hard-core model solutes to structural theories of hydrophobic effects

Hard core models of solute-water interactions studied in this context, which are the basis of scaled-particle theories, are motivated (Pratt, 2002) by the broad success of van der Waals theories of liquids (Barker and Henderson, 1976; Chandler *et al.*, 1983; Lebowitz and Waisman, 1980; Widom, 1967). Physically expressed, van der Waals approaches are appropriate for the description of dense liquids because the disorder and high density can limit structural fluctuations to length-scales associated with the variation of intermolecular repulsive interactions, small compared to the range of intermolecular attractive interactions. When attractive intermolecular interactions are weak on a thermal scale, that helps too since a van der Waal approach treats those interactions perturbatively. Then an approach which separates the effects of intermolecular repulsive and attractive interactions can be successful. In that case, repulsive interactions present the first challenge to theories, and hard-core interactions are natural simple models for those excluded volume interactions. This is the argument for the physical relevance of hard-core model solutes to theories of hydrophobic effects.

With this background, the most important *physical* observation on the large  $R$  behavior of the  $G(R)$  results of Fig. 5 is that those results would be expected to be sensitive to attractive solute-water interactions, if they were to be included. When  $R$  is large, the local density in the vicinity of the hard sphere solute can be low, and the argument above that fluctuations do not access the length-scales comparable to the range of natural attrac-

tive interactions does not apply. Simulation evidence does support the view that results can be sensitive to inclusion of natural attractive interactions when the solution structures have length scales substantially greater than  $R_{\max}$  (Ashbaugh and Paulaitis, 2001; Chau, 2003; Dzubiella and Hansen, 2003; Henderson and van Swol, 1988; Hummer *et al.*, 2001; van Swol and Henderson, 1986; Truskett *et al.*, 2001; Wallqvist *et al.*, 2001; Zhou *et al.*, 2004).

Nevertheless, hard-core models of solute-water interactions serve as an valuable reference point for at least two reasons. A first reason is conceptual and reductionist. This simplified case has historically been considered as expressing the basic puzzle of hydrophobic effects. (The extent to which that is true is one of the issues addressed here!) Solving this basic puzzle enables specific cases to be described by combination of what is understood for the simpler cases. A second reason that hard-core models of solute-water interactions are valuable is that for  $R$  not too large the results should be less sensitive specifically to the case of physical interest. (Support for this view is noted at the appropriate places in the succeeding discussions.) From this point of view, then, the careful study of the large  $R$  behavior of hard sphere  $G(R)$  assists in refining the description of intermediate  $R$  behavior, including the region of the maximum corresponding to the *most hydrophobic* solutes.

### C. Hydration thermodynamics of hydrophobic species: temperature signatures and solubility minima

The hydration free energy of a methane sized ( $R = 3.3 \text{ \AA}$ ) hard-sphere solute in water as a function of temperature along the saturation curve is shown in Fig. 6. The simulation results for the chemical potential pass through a maximum at  $T \approx 400 \text{ K}$ , at which point the hydration entropy defined by  $s_A^{\text{ex}} = -\partial\mu_A^{\text{ex}}/\partial T|_{\text{sat}}$  is zero. To extract the enthalpy and entropy of hydrophobic hydration from the chemical potential, we assume that the heat capacity  $\partial h_A^{\text{ex}}/\partial T|_{\text{sat}} = T\partial s_A^{\text{ex}}/\partial T|_{\text{sat}} = c_A^{\text{ex}}(T)$  is independent of temperature. In this case, the hydration enthalpy, entropy, and free energy are

$$h_A^{\text{ex}} = h_A^{\text{ex}}(T_0) + (T - T_0) c_A^{\text{ex}}(T_0) , \quad (16a)$$

$$s_A^{\text{ex}} = s_A^{\text{ex}}(T_0) + \ln\left(\frac{T}{T_0}\right) c_A^{\text{ex}}(T_0) , \quad (16b)$$

$$\begin{aligned} \mu_A^{\text{ex}} = & \mu_A^{\text{ex}}(T_0) + (T - T_0) (c_A^{\text{ex}}(T_0) - s_A^{\text{ex}}(T_0)) \\ & - T \ln\left(\frac{T}{T_0}\right) c_A^{\text{ex}}(T_0) , \end{aligned} \quad (16c)$$

respectively, and  $\mu_A^{\text{ex}}(T_0) = h_A^{\text{ex}}(T_0) - T_0 s_A^{\text{ex}}(T_0)$ .

The enthalpy and entropy of hydration of the methane-sized hard-sphere solute is shown alongside the fitted free energy in Fig. 6. The hydration entropy is negative and unfavorable at room temperature (Blokzijl and Engberts, 1993; Kauzmann, 1959; Tanford, 1980). With increasing temperature the entropy changes

sign indicative of a positive heat capacity increment. The entropy and heat capacity at  $T = 298 \text{ K}$  for the hard-sphere solute are  $-69.5 \text{ J}/(\text{mol K})$  and  $214 \text{ J}/(\text{mol K})$ , respectively, which is in excellent agreement with the experimental values for the entropy and heat capacity of  $-66.7 \text{ J}/(\text{mol K})$  and  $209$  to  $237 \text{ J}/(\text{mol K})$  for methane at  $T = 298 \text{ K}$  (Ben-Naim and Marcus, 1984; Lazaridis and Paulaitis, 1992; Naghibi *et al.*, 1986; Rettich *et al.*, 1981). Over most of the temperature range considered, the hydration enthalpy is positive and unfavorable for hydration, in disagreement with the experimental enthalpy for methane of  $-11.5 \text{ kJ}/\text{mol}$  at  $T = 298 \text{ K}$ , largely a result of the neglect of attractive interactions with water. The *iceberg* hypothesis of Frank and Evans (Frank and Evans, 1945) suggests that local freezing of water in the vicinity of hydrophobic species contributes to the experimental negative hydration enthalpy. In the case of the methane sized hard sphere though, the hydration enthalpy at  $T = 298 \text{ K}$  is  $5.0 \text{ kJ}/\text{mol}$ , contrary to customary expectations.

The ratio of the chemical potential and  $kT$  dictates the Ostwald solubility.  $-\ln K_{\text{eq}}$  for the methane sized solute in water as a function of temperature is shown in Fig. 7. This quantity passes through a maximum near  $T = 280 \text{ K}$ , corresponding to a minimum in the solubility. This observation is in agreement with information theory (Garde *et al.*, 1999) and equation-of-state (Ashbaugh *et al.*, 2002) models of hard-sphere solubilities that link the solubility minimum to the density maximum at  $T = 277 \text{ K}$  for pure water. The solubility minimum corresponds to the point at which the enthalpy,  $h_A^{\text{ex}} = -T^2\partial(\mu_A^{\text{ex}}/T)/\partial T|_{\text{sat}}$  equals zero. Real nonpolar solutes display solubility minima at temperatures well above the density maximum, largely as a result of attractive interactions between the solute and water. These interactions, not included in the present simulations, can be included approximately by assuming they are proportional to the density of liquid water, as in the van der Waals equation-of-state. The resulting chemical potential is  $\mu_A^{\text{ex}} = [\mu_A^{\text{ex}}]_{\text{HS}} - a_{\text{AW}}\rho_{\text{W}}$  (Garde *et al.*, 1999). The effect of including solute-water interactions on the solubility is shown in Fig. 7. Increasing these interactions systematically shifts the maximum in  $\mu_A^{\text{ex}}/kT$ , out to greater temperatures, in agreement with the experimental observation of solubility minima at higher temperatures.

For the hard-sphere solutes the simulation results have slightly more curvature at temperatures near the solubility minimum than predicted by Eq. (16) [Fig. 7]. While the fit is accurate, the enhanced curvature suggests the heat capacity is not constant as assumed above, but is slightly larger at low temperatures. Indeed this has been observed experimentally (Gill *et al.*, 1985), and is borne out by theoretical models of hydrophobic hydration as well (Ashbaugh *et al.*, 2002; Hummer *et al.*, 2000; Silverstein *et al.*, 2001). Nevertheless, the temperature dependence of the heat capacity is minor, and including it is a complication of secondary importance to the interpretations here. We therefore neglect it in our ther-

modynamic analysis.

Fig. 8 shows how the chemical potential of hard spheres in water as a function of temperature with increasing solute size. In the range of sizes shown, the maximum in the chemical potential shifts from temperatures above  $T = 470$  K, above the window of temperatures simulated, for the 2 Å radius solute to lower temperatures with increasing solute sizes. For cavities not much larger than 12 Å (not shown in figure), the maximum falls below  $T = 260$  K, below the simulation window and the normal freezing point of water. Thus, for molecularly sized cavities, hydrophobic hydration is opposed by a negative entropy, at temperatures below the chemical potential maximum, over most of the range of temperatures simulated. For meso- and macroscopic cavities, however, this trend is reversed and hydration is favored by a positive dissolution entropy but is insoluble as a result of a dominating positive enthalpy (demonstrated in the following section), dictated by the temperature dependence of the surface tension of water.

#### D. Surface area dependence of hydration thermodynamic properties: curvature corrections and a Tolman length

In an effort to compare and correlate hydration free energies of a variety species, it is common to calculate the free energy cost per unit area for hydrating nonpolar solute surfaces, also referred to as a molecular surface tension (Hermann, 1977; Tanford, 1979). This molecular surface tension, however, is generally not equal to the free energy of creating a macroscopic flat interface, in part due to curvature and structural differences between water at molecular and macroscopic interfaces. Nevertheless, SPT systematically interpolates the surface tension between these two length-scale extremes, and provides insight into their relationship (Ashbaugh and Paulaitis, 2001; Huang and Chandler, 2000a; Huang *et al.*, 2001).

Under the assumption that the pressure contribution to the hydration free energy is negligible, an excellent assumption for liquid water, a surface tension for hydration of a hard-sphere solute is obtained from the surface area derivative of the chemical potential (Ashbaugh and Paulaitis, 2001). This derivative depends, however, on the definition of the surface area. A natural choice for the solute area is defined by  $R$ , and is referred to as the solvent accessible surface (SAS) area,  $A_{\text{SAS}} = 4\pi R^2$ . Differentiating the chemical potential with respect to this surface area yields

$$\gamma_{\text{SAS}}(R) = \frac{\partial \mu_{\text{A}}^{\text{ex}}}{\partial 4\pi R^2} = \frac{1}{2} kT \rho_{\text{W}} G(R) R. \quad (17)$$

More generally, the solute surface can be defined by a

radius  $R - \Delta R$ . In this case the surface tension is

$$\begin{aligned} \gamma(R; \Delta R) &= \frac{\partial \mu_{\text{A}}^{\text{ex}}}{\partial [4\pi (R - \Delta R)^2]} = \frac{kT \rho_{\text{W}} G(R) R^2}{2(R - \Delta R)} \\ &= \frac{\gamma_{\text{SAS}}(R)}{1 - \Delta R/R}. \end{aligned} \quad (18)$$

The SAS tension as a function of  $R$  at  $T = 300$  K is shown in Fig. 9. The surface enthalpy,  $\partial h_{\text{A}}^{\text{ex}}(T_0)/\partial A_{\text{SAS}}$ , entropy,  $\partial s_{\text{A}}^{\text{ex}}(T_0)/\partial A_{\text{SAS}}$ , and heat capacity,  $\partial c_{\text{A}}^{\text{ex}}(T_0)/\partial A_{\text{SAS}}$ , are included in this figure. For small cavities, all the surface thermodynamic properties go to zero as  $R \rightarrow 0$ . With increasing size, the surface tension increases monotonically and approaches its asymptotic limit for a flat interface of  $\gamma_{\infty} = 0.432$  kJ/(mol Å<sup>2</sup>) = 71.7 dyne/cm. The other surface properties, most notably the heat capacity, approach their asymptotic plateaus more slowly with increasing  $R$ . Like the surface tension, the surface enthalpy monotonically increases with increasing solute size. The surface entropy and heat capacity, on the other hand, vary in distinctly different ways for molecular and macroscopic surfaces, indicating changes in the mechanism of hydration (Southall and Dill, 2000). In particular, the surface entropy is initially negative beginning from  $R = 0$ , consistent with the experimental thermodynamics of hydrophobic hydration for molecular solutes, reaches a minimum at  $R \approx 3.3$  Å and then increases, eventually becoming positive as expected from the temperature dependence of the liquid-vapor interface. It is curious that the size at this minimum is close to the size of the maximum of  $G(R)$ , that is for the *most hydrophobic* hard sphere solute. While the surface heat capacity is positive over the entire size range, it reaches a maximum at solute radii comparable to the position of the minimum in the entropy, suggesting the two are related. Moreover, we may infer that the maxima in the surface entropy and heat capacity are linked to the breakdown of the aqueous network in the vicinity of the hard-sphere solute as observed in simulation studies linking solute-water correlations to the thermodynamics of hydrophobic hydration (Lazaridis and Paulaitis, 1994).

Sharp and coworkers (Sharp *et al.*, 1991) suggested that rather than relying solely on the SAS to determine the molecular surface tension, this tension needs to be corrected for the curvature of the molecular interface to reconcile the difference between molecular and macroscopic surface tension. Based on geometric arguments, they proposed that the radius of a water molecule is the length-scale over which this correction must be applied. In effect, their work indicates that the van der Waals surface, i.e.,  $\Delta R = \sigma_{\text{WW}}/2 = 1.4$  Å, provides a superior description of molecular solute hydration (Jackson and Sternberg, 1994; Sharp *et al.*, 1991). A schematic illustration of the van der Waals, solvent accessible, and curvature corrected radii of a hard sphere solute in water is given in Fig. 10. For a methane sized solute  $\gamma(R = 3.3\text{Å}; \Delta R = 0.0\text{Å}) = 0.300$

kJ/(mol Å<sup>2</sup>), 30% lower than the macroscopic value, while  $\gamma(R = 3.3\text{Å}; \Delta R = 1.4\text{Å}) = 0.521$  kJ/(mol Å<sup>2</sup>), 20% greater than the macroscopic value. While neither of these two surfaces gives the macroscopic result, they do bracket  $\gamma_\infty$  suggesting there an optimal intermediate value of  $\Delta R$  for which the surface tension is size independent.

Fig. 11 shows how the surface tension varies with  $\Delta R$ . The divergence in  $\gamma(R; \Delta R)$  results from the divergence in Eq. (18) as  $R \rightarrow \Delta R$ . For solutes larger than 2.5 Å, using  $\Delta R = 1$  Å yields a surface tension that is only weakly size dependent. Indeed,  $\gamma(R = 3.3\text{Å}; \Delta R = 1.0\text{Å}) = 0.430$  kJ/(mol Å<sup>2</sup>) is in excellent agreement with the macroscopic value, suggesting that Honig and coworker’s geometric estimate of the curvature correction length-scale is correct. This argument falls apart, however, when we consider the temperature dependence of the Tolman length.

The Tolman length  $\delta$ , described in Sec. II.A, can be accessed by the revised SPT through Eqs. 9 and 17:

$$\gamma_{\text{SAS}}(R) \sim \gamma_\infty \left(1 - \frac{2\delta}{R}\right). \quad (19)$$

Substituting this expression into Eq. (18) yields (Ashbaugh and Paulaitis, 2001)

$$\gamma(R; \Delta R) \sim \gamma_\infty \left(\frac{1 - 2\delta/R}{1 - \Delta R/R}\right) \quad (20)$$

for the surface tension referenced to a surface displaced by  $\Delta R$ . Thus, for large  $R$  the optimal surface for obtaining a size independent surface free energy is  $\Delta R = 2\delta$ . This Tolman length can be calculated from classic SPT, see Eq. 10 in (Stillinger, 1973), and yields an nearly temperature independent  $\delta \approx 0.5$  Å [Fig. 12], in good agreement with the empirical  $\Delta R$  at  $T = 300$  K obtained above. The revised SPT, however, finds that  $\delta$  is strongly temperature dependent. While the classic SPT correctly predicts the magnitude of  $\delta$  at low temperature,  $\delta$  decreases with temperature and changes sign near  $T = 350$  K. Furthermore, (Moody and Attard, 2001) suggest that the Tolman length might change sign also for a Lennard-Jones solvent. Thus assuming the  $\Delta R$  is simply dictated by the size of a water molecule leads to fundamentally flawed interpretations of the relationship between molecular and macroscopic surface tensions (Jackson and Sternberg, 1994; Sharp *et al.*, 1991). In retrospect, the temperature dependence of the curvature correction might have been anticipated by the entropic differences between hydrating a molecular and mesoscopic interface and the significantly different temperature dependencies of the associated surface thermodynamic properties [Fig. 9]. The curves observed in this figure are simply too rich to be described by a temperature independent length-scale.

## E. Entropy convergence and solute size

When the hydrophobic component of the hydration entropies of these molecules is extrapolated to high temperatures, the entropies converge to one another within a narrow range near  $T = 385$  K (Baldwin, 1986; Murphy *et al.*, 1990; Privalov, 1979; Privalov and Gill, 1988). This phenomenon of entropy convergence is feature of hydrophobic hydration believed to be shared between small molecule hydration and protein unfolding thermodynamics. Baldwin and Privalov noted that this can result from proportionality of the entropy and heat capacity of hydration to one another. The most successful explanations for the convergence temperature for small molecules have related the convergence temperature to the equation-of-state of pure water (Ashbaugh *et al.*, 2002; Garde and Ashbaugh, 2001; Garde *et al.*, 1996; Hummer *et al.*, 1998). (Huang and Chandler, 2000b) argued that for species larger than  $R \approx 10$  Å entropy convergence does not occur, and therefore proteins do not exhibit this phenomenon.

In Fig. 13 we have plotted the hydration entropies for hard-sphere solutes as a function of temperature for solutes in the size range  $2 \text{ Å} \leq R \leq 10 \text{ Å}$ . Indeed, there is a broad range of convergence temperatures observed at each point where an entropy curve, for a given size, crosses that for another solute. For example, the 2 Å solute entropy intersects the 3 Å solute entropy at  $T = 410$  K, while the 2 Å solute entropy intersects the 10 Å solute curve at  $T = 300$  K, indicating that there is no unique convergence temperature. Experimental identifications of that entropy convergence, however, have largely concerned themselves with solutes similar in size. We therefore consider how the convergence temperature changes with differential perturbations in the solute size. In this case, convergence occurs at the temperature for which  $\Delta s_A^{\text{ex}}(R \rightarrow R + \delta R) = 0$ . Assuming the hydration heat capacity is independent of temperature,  $T_c$  is determined by the relationship

$$T_c = T_0 \exp\left(-\frac{\partial s_A^{\text{ex}}(T_0)}{\partial A_{\text{SAS}}} / \frac{\partial c_A^{\text{ex}}(T_0)}{\partial A_{\text{SAS}}}\right) \quad (21)$$

with a size dependence dictated by the relationship between  $\partial s_A^{\text{ex}}(T_0)/\partial A_{\text{SAS}}$  and  $\partial c_A^{\text{ex}}(T_0)/\partial A_{\text{SAS}}$  on the solute radius in Fig. 9. The differential entropy convergence temperature curve determined by these expressions is shown in Fig. 13. Two points of interest are immediately apparent: first the convergence entropy is negative and becomes more negative with increasing solute size, second the convergence entropy curve more or less forms a lower bound on the hydration entropy as a function of temperature, although this is approximate.

One of the implications of Eq. (21) is that if the entropy is a linear function of the heat capacity, *i.e.*,  $s^{\text{ex}}(T_0) = mc^{\text{ex}}(T_0) + b$ , as suggested by (Baldwin, 1986; Murphy *et al.*, 1990), then the convergence temperature would be independent of solute size. In Fig. 14 we see

that  $T_c$  has a significant solute size dependence, indicating that this assumption has limited validity. For solutes approaching zero radius,  $T_c$  plateaus at a maximum. With increasing solute size  $T_c$  decreases so that above  $R \approx 8 \text{ \AA}$  it is less than the normal freezing point of water. At the intermediate methane radius of  $3.3 \text{ \AA}$ , however, the convergence temperature is  $382\text{K}$  in excellent agreement with the experimental convergence temperature of  $T = 385 \text{ K}$  for simple nonpolar gases and linear alkanes.

We note that the convergence temperature as  $R \rightarrow 0$  plateaus at  $T = 655 \text{ K}$ , above the critical temperature of water at  $647 \text{ K}$ . This unphysical result is due, in part, to our extrapolation of the entropies beyond the range,  $260 \text{ K}$  to  $470 \text{ K}$ , to which we fitted Eq. (16). For cavities small enough that only one water molecule can fit inside, the free energy is given by Eq. (6), and entropy convergence occurs for the temperature at which

$$\alpha_{\text{sat}} T_c = 1 - \frac{4\pi}{3} \rho_{\text{W}} R^3, \quad (22)$$

where  $\alpha_{\text{sat}} = -(\partial \ln \rho_{\text{W}} / \partial T)_{\text{sat}}$  is the thermal expansion coefficient of liquid water along the saturation curve. When this criterion is applied, it displays a plateau at a physically more realistic temperature of  $T_c \approx 525 \text{ K}$  [Fig. 14]. With increasing solute size, Eq. (22) indicates a sudden decrease in  $T_c$  above  $R \approx 1 \text{ \AA}$ , comparable to that obtained on the assumption that the heat capacity is temperature independent. Above radii of  $1.25 \text{ \AA}$ , Eq. (22) breaks down as multi-particle correlations began to play a role in the solute entropy. At this radius, however, the convergence temperatures are now within the range of temperatures simulated and the application of Eq. (21) becomes more accurate. It is reasonable then to interpolate between the convergence temperatures determined by Eq. (21) and Eq. (22), as indicated in Fig. 14.

We note that the information theory (Garde *et al.*, 1996; Hummer *et al.*, 1998), with natural simplifying assumptions, indicates entropy convergence when  $T_c \approx (2\alpha_{\text{sat}})^{-1} = 420 \text{ K}$ . This corresponds on Fig. 14 to a solute radius of  $R \approx 2.1 \text{ \AA}$  placing this estimate among small-solute theories. Relaxing the assumptions used to arrive at this IT criterion lowers the convergence temperature prediction for methane sized solutes to  $T \approx 390 \text{ K}$ , improving agreement with the present result of  $382 \text{ K}$ .

The apparent convergence of the entropy change at  $T = 385 \text{ K}$  to a value close to zero for a range of hydrophobic solutes and proteins has suggested that the hydration of these chemically distinct solutes are related (Baldwin, 1986; Murphy *et al.*, 1990). Assuming that the temperature dependence for protein unfolding arises solely from the exposure of hydrophobic side chains to water, phenomenological models have been developed which separate out residual temperature independent components of the entropy, from contributions such as changes in the chain conformation, by extrapolating to the convergence temperature. This procedure relies, in part, on the assumption that the hydration of surface

hydrophobic groups is the same in the native and denatured conformations, and therefore cancels in the entropy difference.

The surprising explanation of the entropy convergence phenomena that tied it to the particular equation of state of liquid water (Ashbaugh *et al.*, 2002; Garde and Ashbaugh, 2001; Garde *et al.*, 1996; Hummer *et al.*, 1998) resolved an important conundrum for our molecular understanding of hydrophobic effects. Whether and how this entropy convergence phenomena is involved with protein *folding* is yet an outstanding question. Proteins are complicated molecules participating in both hydrophobic and hydrophilic interactions with the solution. The widely appreciated point that protein folding thermodynamics may be primarily sensitive to hydration of unfolded configurations is just as important (Paulaitis and Pratt, 2002; Pratt and Pohorille, 2002). Considering unfolded possibilities, the sizes of the obvious hydrophobic units are in the range of small molecule hydrocarbon solutes. The largest hydrophobic side chain —phenyl alanine— is an example. (Pratt, 2002) emphasized that solution thermodynamic data are available for hydrophobic solutes of just this size, *e.g.* for benzene, toluene, and ethyl benzene (Privalov and Gill, 1989), and those data suggest that these solutes exhibit conventional entropy convergence behavior. Thus, it is a plausible hypothesis that entropy convergence will be expressed in protein folding thermodynamics primarily through contributions associated with the unfolded configurations.

(Huang and Chandler, 2000b) suggested that the hydration of surface nonpolar groups is better described by the hydration entropy of a solute surface comparable in size to the protein radius on the order of tens of angstroms, rather than treating the surface groups individually as having sizes comparable to simple hydrophobic units. In this hypothesis it is presumed that entropic contributions for hydrating large hydrophobic surfaces with attractive dispersion interactions and vicinal polar/charged groups is the same as that for a hard repulsive surface. Recent simulations of convex methane clusters have found that when realistic attractive interactions between water and methane are included, water packs around the cluster methane sites just as it does around a solitary methane in solution (Ashbaugh and Paulaitis, 2001; Chau, 2003). Moreover, Cheng and Rossky (Cheng and Rossky, 1998) found that the orientational correlations between water and proximal hydrophobic residues on the convex surfaces of the bee venom protein, meletin, are comparable to those near individual solitary hydrophobic groups in solution. These observations suggest that the available configurational space, and by extension the entropy, for water molecules near realistic surface hydrophobic units is the same in the folded and unfolded states, supporting the assumptions of the phenomenological folding models. We note, however, that in the same study Cheng and Rossky found that water molecules proximal to hydrophobic

residues in flat portions of meletin were more orientationally disordered as a result of the difficulties associated with maintaining the aqueous hydrogen-bonding network near restrictive solute topologies (Cheng and Rosky, 1998). Thus, the applicability of the phenomenological unfolding model may be complicated by the protein surface topography and the impact of hydrophobic pockets on the overall unfolding entropy. This can introduce further scatter into measured folding entropies (Robertson and Murphy, 1997).

#### IV. SUMMARY AND CONCLUSIONS

The revised scaled-particle theory bridges the known molecular and macroscopic limits by utilizing simulation information on multi-body correlations in liquid water together with experimental thermodynamic properties of pure water to construct a functional form for the hydration free energy of hydrophobic hard-sphere solutes in water. The classic scaled-particle theory (Ben-Naim and Friedman, 1967; Mayer, 1963; Stillinger, 1973) incorrectly predicts an increase in the surface tension of water with increasing temperature, and a suspiciously temperature independent Tolman length which does not agree with revised scaled-particle theory observations. As a result, application of classic scaled-particle theory to hydration free energies is largely a fitting exercise to obtain the effective van der Waals diameter,  $\sigma_{ww}$ , of water. Conclusions drawn from this tack have weak significance regarding the molecular origins of the hydrophobic effect, and are limited to comparisons of the size parameter for water relative to other solvents, neglecting further molecular detail or specific temperature signatures of hydrophobic hydration.

The revised scaled-particle theory is more successful, but the success of the scaled particle approach derives generally from the remarkable fact that the results identify a molecular length, near 3.0 Å, that provides a good joining point for microscopic and macroscopic descriptions. The corresponding results for comparative organic solvents are less simple (Graziano, 2003; Pratt and Pohorille, 1992). That micro-macro joining radius exhibits interesting temperature variation; an accurate description of those temperature variations is an important part of the higher fidelity of the revised scaled-particle results. The revised scaled-particle theory reproduces the solubility minimum behavior for small hydrophobic solutes, and demonstrates significant changes in the hydration mechanism of hard-sphere solutes with increasing solute size. Specifically, the hydration thermodynamics of small solutes is predominantly entropic at room temperature, but the hydration of mesoscopic cavities is entropically favorable and opposed by a dominating hydration enthalpy. While it is tempting to describe these changes in hydration thermodynamics in terms of aqueous hydrogen-bonding near the hydrophobic entity — and that can be plausible in the appropriate theoret-

ical setting — the scaled-particle theory provides little in the way of information on the integrity of hydrogen bonded networks.

Nevertheless, the revised scaled-particle theory does provide thermodynamic information that challenges phenomenological views of hydrophobic effects, particularly the cherished *iceberg* hypothesis. Whereas the iceberg hypothesis suggests that local freezing of water molecules in the vicinity of hydrophobic solutes is a source for the negative hydration enthalpies, we find that at room temperature the hydration of solutes comparable in size to simple nonpolar gases is actually unfavorable from an enthalpic as well as an entropic standpoint. The experimentally determined favorable enthalpies of solution of hydrophobic species then are a consequence of attractive solute-water interactions and not enhanced water-water structuring.

On a molecular level there is a surface that maps macroscopic surface tensions to molecular values. This reduces the reconciliation of molecular and macroscopic values of the surface tension to a program of finding the appropriate dividing surface. The utility of that program rests on the optimistic expectation that the Tolman length is largely temperature independent. But that the Tolman length was found to have a significant temperature dependence in water, changing from positive to negative at  $T \approx 350$  K, a possibility anticipated by Stillinger (Stillinger, 1973). As a result then, though the optimal surface for the description of hydration may be approximated by the solute molecular surface at low temperatures (Ashbaugh *et al.*, 1999; Ashbaugh and Paulaitis, 2001), with increasing temperature this optimized surface moves out to the solvent accessible surface at  $T \approx 350$  K, and ultimately extends beyond this surface at even higher temperatures as a result of the nontrivial temperature dependence of the hydration thermodynamics for molecular-sized solutes.

Finally, the revised scaled-particle theory provides detailed information on the curious entropy convergence behavior observed for small molecule solutes and the size dependence of the convergence temperature. A suitably defined entropy convergence temperature retreats below the freezing temperature of water for hard spheres the size of globular soluble proteins. But heterogeneity of protein-water interactions and of sizes of hydrophobic units also contribute importantly to experimental blurring of entropy convergence behavior in protein unfolding thermodynamic data. Equally important, entropy convergence behavior for protein *folding* thermodynamics may be primarily expressed through contributions associated with the unfolded configurations, and due to hydration of hydrophobic side chains of size corresponding to studied small molecule solutes.

## Acknowledgements

This work was supported by the U. S. Department of Energy, contract E-7405-ENG-36. HSA acknowledges support from a Los Alamos Director's Fellowship. This research has benefited from conversations with D. Asthigiri, A. E. García, S. Garde, G. Hummer, M. E. Paulaitis, and A. Pohorille. We also thank J. R. Henderson and R. Evans for their insightful remarks with respect to the wetting of interfaces.

## References

- Alejandre, J., D. J. Tildesley, and G. A. Chapela, 1995, *J. Chem. Phys.* **102**, 4574.
- Ashbaugh, H. S., D. Asthagiri, L. R. Pratt, and S. B. Rempe, 2003, *Biophys. Chem.* **105**, 323.
- Ashbaugh, H. S., E. W. Kaler, and M. E. Paulaitis, 1999, *J. Am. Chem. Soc.* **121**, 9243.
- Ashbaugh, H. S., and M. E. Paulaitis, 1996, *J. Phys. Chem.* **100**, 1900.
- Ashbaugh, H. S., and M. E. Paulaitis, 2001, *J. Am. Chem. Soc.* **123**, 10721.
- Ashbaugh, H. S., L. R. Pratt, M. E. Paulaitis, J. Clohery, and T. L. Beck, 2004, *Deblurred Observation of the Molecular Structure of a Water-Oil Interface*, Technical Report LA-UR-04-4750, Los Alamos National Laboratory.
- Ashbaugh, H. S., T. M. Truskett, and P. G. Debenedetti, 2002, *J. Chem. Phys.* **116**, 2907.
- Baldwin, R. L., 1986, *Proc. Natl. Acad. Sci. USA* **83**, 8069.
- Barker, J. A., and D. Henderson, 1976, *Rev. Mod. Phys.* **48**, 587.
- Ben-Naim, A., and H. L. Friedman, 1967, *J. Phys. Chem* **71**, 448.
- Ben-Naim, A., and Y. Marcus, 1984, *J. Chem. Phys.* **81**, 2016.
- Berendsen, H. J. C., J. R. Grigera, and T. P. Straatsma, 1987, *J. Phys. Chem.* **91**, 6269.
- Blokzijl, W., and J. B. F. N. Engberts, 1993, *Angew. Chem. Int. Ed. Engl.* **32**, 1545.
- Bowron, D. T., A. Filipponi, C. Lobban, and J. L. Finney, 1998a, *Chem. Phys. Letts.* **293**, 33.
- Bowron, D. T., A. Filipponi, M. A. Roberts, and J. L. Finney, 1998b, *Phys. Rev. Lett.* **81**, 4164.
- Brandts, J. F., 1964, *J. Am. Chem. Soc.* **86**, 4291.
- Broadbent, R. D., and G. W. Neilson, 1994, *J. Chem. Phys.* **100**, 7543.
- Chandler, D., 1993, *Phys. Rev. E* **48**, 2898.
- Chandler, D., J. D. Weeks, and H. C. Andersen, 1983, *Science* **220**, 787.
- Chau, P. L., 2003, *Mol. Phys.* **101**, 3121.
- Chen, L. J., S. Y. Lin, and C. C. Huang, 1998a, *J. Phys. Chem. B* **102**, 4350.
- Chen, L. J., S. Y. Lin, C. C. Huang, and E. M. Chen, 1998b, *Colloids Surf. A* **135**, 175.
- Cheng, Y. K., and P. J. Rossky, 1998, *Nature* **392**, 696.
- Christenson, H. K., and P. M. Claesson, 1988, *Science* **239**, 390.
- Considine, R. F., R. A. Hayes, and R. G. Horn, 1999, *Langmuir* **15**, 1657.
- DeJong, P. H. K., J. E. Wilson, G. W. Neilson, and A. D. Buckingham, 1997, *Mol. Phys.* **91**, 99.
- Dzubiella, J., and J. P. Hansen, 2003, *J. Chem. Phys.* **119**, 12049.
- Egelstaff, P. A., and B. Widom, 1970, *J. Chem. Phys.* **53**, 2667 .
- Evans, R., J. R. Henderson, and R. Roth, 2004, *J. Chem. Phys.* **121**, 12074 .
- Evans, R., R. Roth, and P. Bryk, 2003, *Europhys. Letts.* **62**, 815.
- Filipponi, A., D. T. Bowron, C. Lobban, and J. L. Finney, 1997, *Phys. Rev. Letts.* **79**, 1293.
- Frank, H. S., and M. W. Evans, 1945, *J. Chem. Phys.* **13**, 507.
- Franks, F., and R. H. M. Hatley, 1991, *Pure Appl. Chem.* **63**, 1367.
- Frenkel, D., and B. Smit, 2002, *Understanding Molecular Simulation. From Algorithms to Applications* (Academic Press, San Diego), 2nd edition.
- Galicchio, E., M. M. Kubo, and R. M. Levy, 2000, *J. Phys. Chem. B* **104**, 6271 .
- Garde, S., and H. S. Ashbaugh, 2001, *J. Chem. Phys.* **115**, 977.
- Garde, S., A. E. García, L. R. Pratt, and G. Hummer, 1999, *Biophys. Chem.* **78**, 21.
- Garde, S., G. Hummer, A. E. García, M. E. Paulaitis, and L. R. Pratt, 1996, *Phys. Rev. Letts.* **77**, 4966.
- Gill, S. J., S. F. Dec, G. Olofsson, and I. Wadso, 1985, *J. Phys. Chem.* **89**, 3758.
- Gomez, M. A., L. R. Pratt, G. Hummer, and S. Garde, 1999, *J. Phys. Chem. B* **103**, 3520.
- Graziano, G., 2003, *Biophys. Chem.* **104**, 393.
- Hare, D. E., and C. M. Sorensen, 1986, *J. Chem. Phys.* **84**, 5085 .
- Henderson, J. R., 2002, *J. Chem. Phys.* **116**, 5039.
- Henderson, J. R., and F. van Swol, 1988, *J. Chem. Phys.* **89**, 5010 .
- Hermann, R. B., 1977, *Proc. Natl. Acad. Sci. USA* **74**, 4144.
- Huang, D. M., and D. Chandler, 2000a, *Phys. Rev. E* **61**, 1501.
- Huang, D. M., and D. Chandler, 2000b, *Proc. Natl. Acad. Sci. USA* **97**, 8324 .
- Huang, D. M., P. L. Geissler, and D. Chandler, 2001, *J. Phys. Chem. B* **105**, 6704 .
- Huang, X., C. J. Margulis, and B. J. Berne, 2003, *Proc. Nat. Acad. Sci. USA* **100**, 11953 .
- Hummer, G., and S. Garde, 1998, *Phys. Rev. Letts.* **80**, 4193.
- Hummer, G., S. Garde, A. E. García, M. E. Paulaitis, and L. R. Pratt, 1998, *J. Phys. Chem. B* **102**, 10469.
- Hummer, G., S. Garde, A. E. García, A. Pohorille, and L. R. Pratt, 1996, *Proc. Natl. Acad. Sci. USA* **93**, 8951.
- Hummer, G., S. Garde, A. E. García, and L. R. Pratt, 2000, *Chem. Phys.* **258**, 349.
- Hummer, G., J. C. Rasaiah, and J. P. Noworyta, 2001, *Nature* **414**(6860), 188.
- Hura, G., D. Russo, R. M. Glaeser, T. Head-Gordon, M. Krack, and M. Parrinello, 2003, *PCCP* **5**, 1981 .
- Israelachvili, J., and R. Pashley, 1982, *Nature* **300**, 341.
- Jackson, R. M., and M. J. E. Sternberg, 1994, *Prot. Eng.* **7**, 371.
- Kauzmann, W., 1959, *Adv. Protein Chem.* **14**, 1.
- Kokkoli, E., and C. F. Zukoski, 1998, *Langmuir* **14**, 1189.
- Lazaridis, T., 2001, *Acc. Chem. Res.* **34**, 931.
- Lazaridis, T., and M. E. Paulaitis, 1992, *J. Phys. Chem.* **96**, 3847.
- Lazaridis, T., and M. E. Paulaitis, 1994, *J. Phys. Chem.* **98**,

- 635 .
- Lebowitz, J. L., and E. M. Waisman, 1980, *Physics Today* **33**, 24.
- Lee, B., 1985, *Biopolymers* **24**, 813.
- Lee, B., 1991, *Proc. Natl. Acad. Sci. USA* **88**, 5154.
- Lum, K., D. Chandler, and J. D. Weeks, 1999, *J. Phys. Chem. B* **103**, 4570.
- Makhatadze, G. I., and P. L. Privalov, 1995, *Adv. Protein Chem.* **47**, 307.
- Mayer, S. W., 1963, *J. Phys. Chem.* **67**, 2160 .
- Moody, M. P., and P. Attard, 2001, *J. Chem. Phys.* **115**, 8967.
- Muller, N., 1993, *Biopolymers* **33**, 1185.
- Murphy, K. P., P. L. Privalov, and S. J. Gill, 1990, *Science* **247**, 559.
- Naghibi, H., S. F. Dec, and S. J. Gill, 1986, *J. Phys. Chem.* **90**, 4621 .
- Pashley, R. M., 2003, *J. Phys. Chem. B* **107**, 1714.
- Pashley, R. M., P. M. McGuiggan, B. W. Ninham, and D. F. Evans, 1985, *Science* **229**, 1088.
- Pashley, R. M., M. Rzechowicz, L. R. Pashley, and M. J. Francis, 2004, *J. Phys. Chem. B* .
- Paulaitis, M. E., and L. R. Pratt, 2002, in *Advances in Protein Chemistry: Unfolded Proteins* (Academic Press), volume 62, p. 283.
- Pierotti, R. A., 1976, *Chem. Rev.* **76**, 717.
- Pohorille, A., and L. R. Pratt, 1990, *J. Am. Chem. Soc.* **112**, 5066.
- Pollack, G. L., 1991, *Science* **251**, 1323.
- Pratt, L., G. Hummer, and S. Garde, 1999, in *New Approaches to Problems in Liquid State Theory*, edited by C. Caccamo, J.-P. Hansen, and G. Stell (Kluwer, Netherlands), volume 529 of *NATO Science Series*, pp. 407–420.
- Pratt, L. R., 1998, in *Encyclopedia of Computational Chemistry* (John Wiley & Sons, Chichester), p. 1286.
- Pratt, L. R., 2002, *Annu. Rev. Phys. Chem.* **53**, 409.
- Pratt, L. R., and D. Chandler, 1977, *J. Chem. Phys.* **67**, 3863.
- Pratt, L. R., and A. Pohorille, 1992, *Proc. Natl. Acad. Sci. USA* **89**, 2995.
- Pratt, L. R., and A. Pohorille, 1993, in *Proceedings of the EBSA 1992 International Workshop on Water-Biomolecule Interactions*, edited by M. U. Palma, M. B. Palma-Vittorelli, and F. Parak (Società Italiana de Fisica, Bologna), p. 261.
- Pratt, L. R., and A. Pohorille, 2002, *Chem. Rev.* **102**, 2671.
- Privalov, P. L., 1979, *Adv. Prot. Chem.* **33**, 167.
- Privalov, P. L., and S. J. Gill, 1988, *Adv. Prot. Chem.* **39**, 191.
- Privalov, P. L., and S. J. Gill, 1989, *Pure & Appl. Chem.* **61**, 1097.
- Reiss, H., 1965, *Adv. Chem. Phys.* **9**, 1.
- Reiss, H., 1977, in *Statistical Mechanics and Statistical Methods in Theory and Application*, edited by U. Landman (Plenum, New York), pp. 99–138.
- Reiss, H., H. L. Frisch, and J. L. Lebowitz, 1959, *J. Chem. Phys.* **31**, 369.
- Rettich, T. R., Y. P. Handa, R. Battino, and E. Wilhelm, 1981, *J. Phys. Chem.* **85**, 3230 .
- Robertson, A. D., and K. P. Murphy, 1997, *Chem. Rev.* **97**, 1251.
- Scatena, L. F., M. G. Brown, and G. L. Richmond, 2001, *Science* **292**, 908.
- Sharp, K. A., A. Nichols, R. F. Fine, and B. Honig, 1991, *Science* **252**, 106.
- Silverstein, K. A. T., K. A. Dill, and A. D. J. Haymet, 2001, *J. Chem. Phys.* **114**, 6303.
- Simonson, T., 2003, *Rep. Prog. Phys.* **66**, 737.
- Southall, N. T., and K. A. Dill, 2000, *J. Phys. Chem. B* **104**, 1326.
- Spolar, R. S., J. H. Ha, and M. T. Record, 1989, *Proc. Nat. Acad. Sci. USA* **86**, 8382 .
- Spolar, R. S., and M. T. Record, 1994, *Science* **263**, 777.
- Stell, G., 1985, in *The Wonderful World of Stochastics A Tribute to Elliot W. Montroll*, edited by M. F. Shlesinger and G. H. Weiss (Elsevier Science Publishers, NY), volume XII of *Studies in Statistical Mechanics*, pp. 127–156.
- Stillinger, F. H., 1973, *J. Soln. Chem.* **2**, 141.
- Stillinger, F. H., and M. A. Cotter, 1971, *J. Chem. Phys.* **55**, 3449.
- van Swol, F., and J. R. Henderson, 1986, *J. Chem. Soc. - Faraday Trans. II* **82**, 1685 .
- Tanford, C., 1979, *Proc. Nat. Acad. Sci. USA* **76**, 4175.
- Tanford, C., 1980, *The Hydrophobic Effect: Formation of Micelles and Biological Membranes* (John Wiley & Sons, New York), 2nd edition.
- Tolman, R. C., 1949, *J. Chem. Phys.* **17**, 333.
- Truskett, T. M., P. G. Debenedetti, and S. Torquato, 2001, *J. Chem. Phys.* **114**, 2401.
- Wallqvist, A., E. Gallicchio, and R. M. Levy, 2001, *J. Phys. Chem. B* **105**, 6745 .
- Weeks, J. D., K. Katsov, and K. Vollmayr, 1998, *Phys. Rev. Letts.* **81**, 4400.
- Widom, B., 1967, *Science* **157**(3787), 375.
- Widom, B., 1982, *J. Phys. Chem.* **86**, 869.
- Zhou, R. H., X. H. Huang, C. J. Margulis, and B. J. Berne, 2004, *Science* **305**, 1605 .

Figures

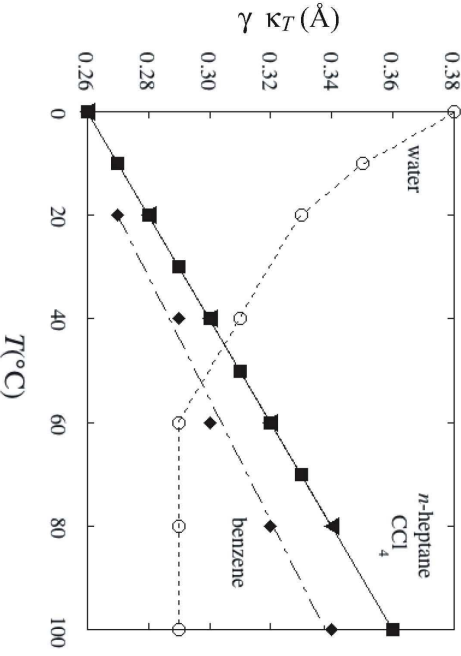


FIG. 1 Product of the liquid-vapor surface tension,  $\gamma$ , and the the isothermal compressibility,  $\kappa_T \equiv -\frac{1}{V} \left( \frac{\partial V}{\partial p} \right)_T$ , for several liquid solvents at low temperatures so that the density of the coexisting vapor is low. Even though the individual factors differ substantially in magnitude, this product is a length characteristic of the liquid, accessible on the basis of macroscopic measurements, and can be taken as proportional to a molecular correlation length. The interesting observation here is that temperature dependence of this correlation length is qualitatively different for liquid water than for these organic solvents.

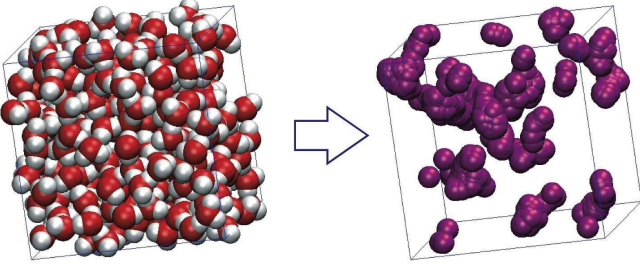


FIG. 2 The box on the left shows a configuration of water molecules taken from a simulation of liquid water at the density of the liquid in coexistence with vapor at 300 K. The box on the right shows hard spheres of diameter 2.8  $\text{\AA}$  that can be successfully placed into the configuration on the right without overlap of the van der Waals volume of the water molecules. The insertion probability  $p_0$  is determined as the volume accessible to centers of the purple spheres divided by the geometric volume of the box.

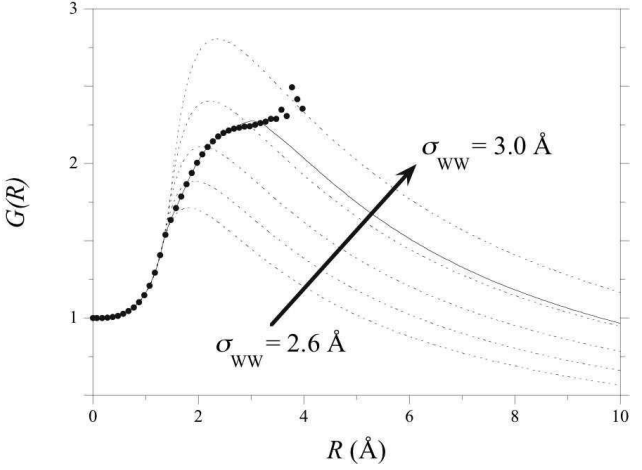


FIG. 3 Cavity contact function for water at  $T = 300$  K at the liquid saturation conditions. The points are obtained by differentiation of the simulation cavity insertion probabilities. The dashed lines are obtained from Reiss’s original SPT theory predictions for a hard sphere solvent, Eq. (10), using effective water hard sphere diameters between  $\sigma_{ww} = 2.6$   $\text{\AA}$  to 3.0  $\text{\AA}$  in 0.1  $\text{\AA}$  increments. The solid line is obtained by differentiation of the revised SPT, Eq. (15), fitted to the simulation results between  $R_{sim} = 2.5$   $\text{\AA}$  and  $R_{macro} = 3.5$   $\text{\AA}$ .

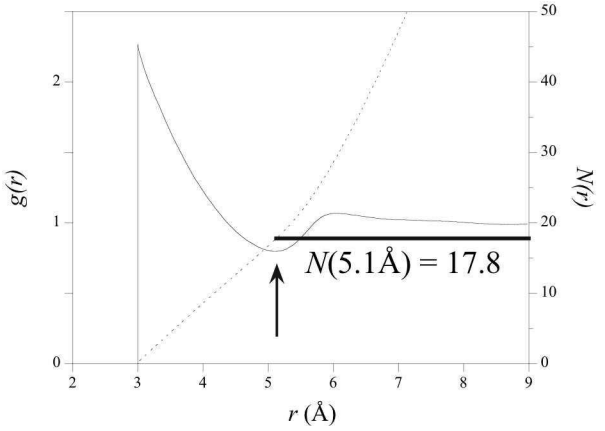


FIG. 4 Cavity-water oxygen radial distribution function for a 3 Å cavity at  $T = 300$  K. The thin solid line indicates the radial distribution function, while the dashed line indicates the radial integral  $N(r) = \int_0^r \rho_w g(\lambda) 4\pi\lambda^2 d\lambda$ . The occupation of the first hydration shell, corresponding to the first minimum in  $g(r)$  at 5.1 Å, is 17.8 water molecules as indicated by the thick horizontal line. Note that the first minimum, which physically discriminates between first and succeeding hydration shells, is mild, and structuring of outer hydration shells is weak (Pratt and Pohorille, 1993). These features are in good qualitative agreement with the predictions of the Pratt-Chandler theory (Pratt and Chandler, 1977), though that specific theory has been substantially amended (Pratt, 2002).

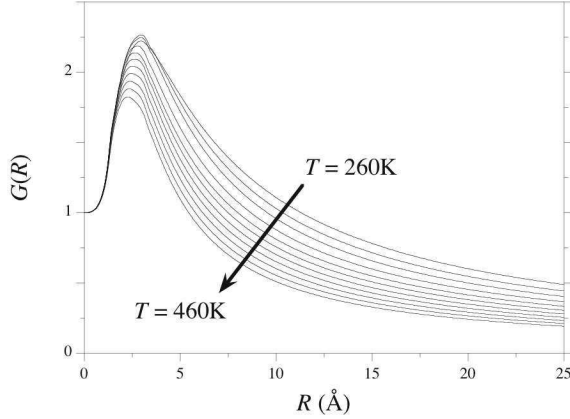


FIG. 5 Cavity contact function for water as a function of temperature along the liquid saturation curve determined by the revised SPT, Eq. (14), with  $R_{\text{sim}} = 2.5$  Å and  $R_{\text{macro}} = 3.5$  Å. Results are shown between  $T = 260$  K to 460 K in 20 K increments. Notice that the length defined by the maximum of this curve *decreases* with decreasing density following increasing temperature along the saturation curve. This is consistent with the suggestion of Fig. 1.

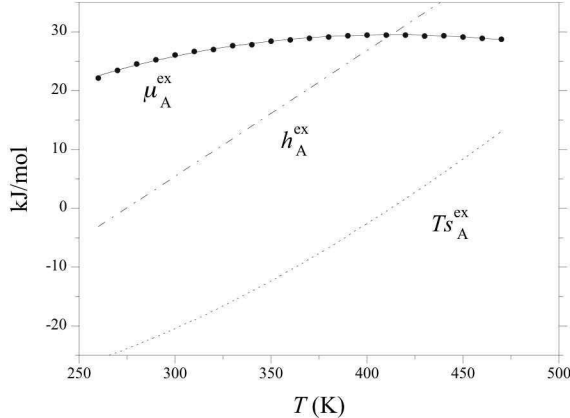


FIG. 6 Excess chemical potential, enthalpy, and entropy of a methane sized hard sphere solute ( $R = 3.3$  Å) in water as a function of temperature along the saturation curve. The points are the explicit simulation results for the chemical potential. Error bars are comparable in size to the points. The curves for the excess chemical potential, enthalpy, and entropy are labeled in the figure. The curves were determined under the assumption that the heat capacity is independent of temperature [Eqs. (16)].

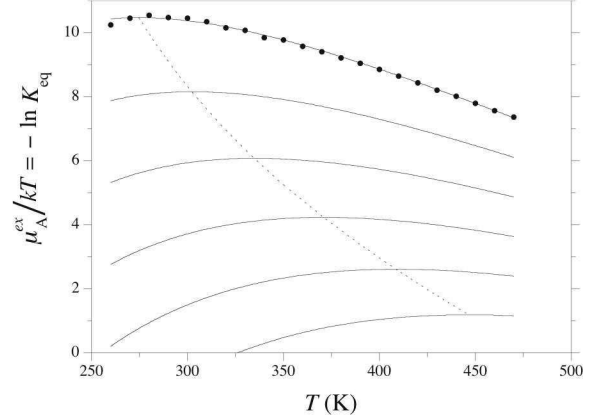


FIG. 7 Solubility of a 3.3 Å *hard-core + weak attractions* solute as a function of temperature with increasing strength of attractive interactions modeled as in the van der Waals equation-of-state,  $\mu_A^{\text{ex}} = [\mu_A^{\text{ex}}]_{\text{HS}} - a_{\text{SW}}\rho_w$ . The points are simulation results from particle insertion probabilities. The solid curves are the solubilities with lower curves indicating increasing attractive interactions,  $a_{\text{SW}} \geq 0$ . The dashed curve indicates the maxima in  $\mu_A^{\text{ex}}/kT$  with increasing interactions, corresponding to minima in the Ostwald solubility, defined as  $K_{\text{eq}} = \exp[-\mu_A^{\text{ex}}(\text{aq})/kT]$  [Eq. (2)].

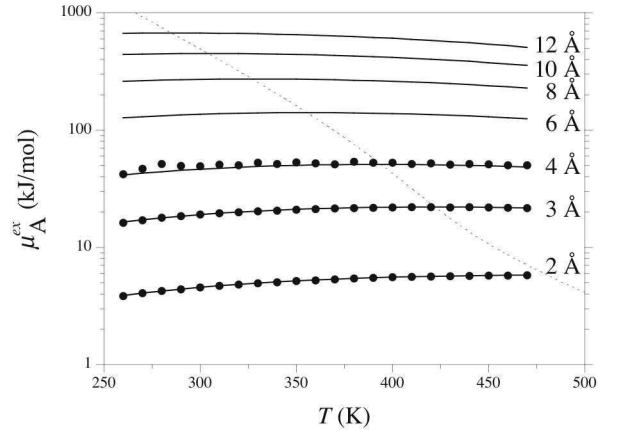


FIG. 8 Excess solute chemical potential as a function of temperature for solutes of varying size. The solid lines correspond to the revised SPT model. The solid circles, open circles, and crosses correspond to explicit molecular simulation results simulation results for the 2 Å, 3 Å, and 4 Å radius solutes, respectively. Estimated statistical errors are smaller than the plotting symbols. The dashed line indicates the locus of chemical potential maxima, where  $s_A^{\text{ex}} = 0$ , with changing cavity size.

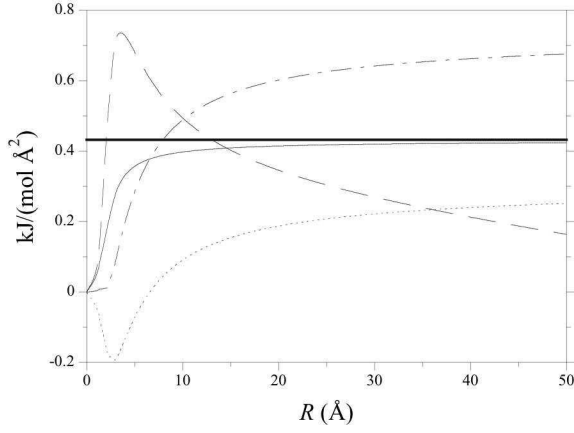


FIG. 9 SAS area derivatives of the hard-sphere solute hydration thermodynamics as a function of solute radius at  $T = 300$  K. The thin solid, long-short dashed, and short dashed, and long dashed lines correspond to  $\partial\mu_A^{\text{ex}}/\partial A_{\text{SAS}}$ ,  $\partial h_A^{\text{ex}}/\partial A_{\text{SAS}}$ ,  $T\partial s_A^{\text{ex}}/\partial A_{\text{SAS}}$ ,  $T\partial c_A^{\text{ex}}/\partial A_{\text{SAS}}$ , respectively. The thick horizontal line indicates the macroscopic surface tension for a flat surface.

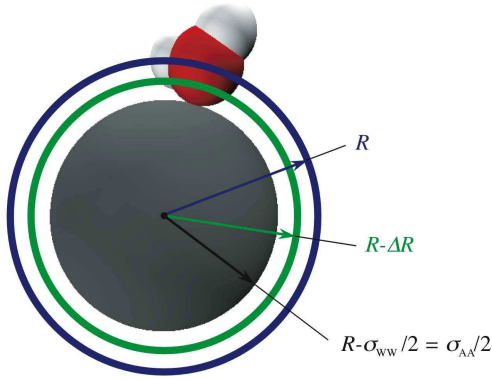


FIG. 10 Alternative definitions of the radius of a hard sphere cavity. The solvent accessible radius,  $R$ , is given by the distance of closest approach between the center of the cavity and the water oxygen center. The radius  $R - \sigma_{\text{WW}}/2$  demarks the van der Waals boundary of the cavity at  $\sigma_{\text{AA}}/2$ .  $R - \Delta R$  locates a neighboring surface that might provide a curvature corrected surface tension.

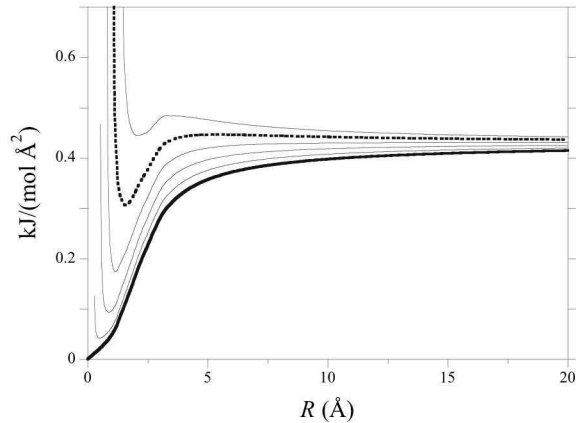


FIG. 11 Surface tension for hydration of hard-sphere solutes as a function of solute radius at  $T = 300$  K employing different definitions of the solute surface. The thick solid line corresponds to the surface tension determined by the derivative with respect to the solvent accessible surface area defined by the radius  $R$  [Eq. (17)]. The lines above the baseline SAS surface tension indicate the effect of increasing  $\Delta R$  in  $0.25$  Å increments from  $0.25$  Å to  $1.25$  Å [Eq. (18)]. The thick dashed line corresponds to  $\Delta R = 1$  Å.

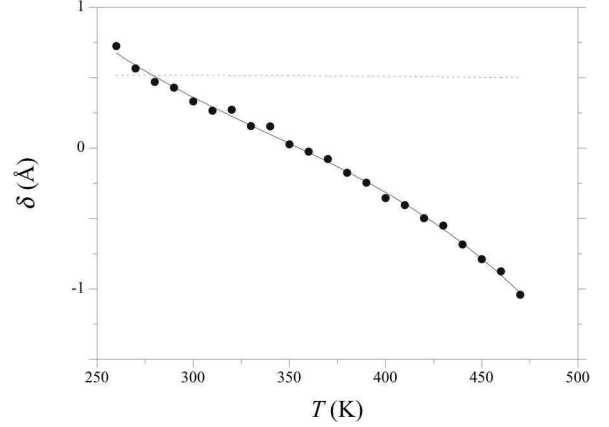


FIG. 12 The curvature correction,  $\delta$ , as a function of temperature along the saturation curve of water. The points correspond to the values determined by the fit of Eq. (14) to the simulation free energies. The solid line is a guide to the eye for the fitted results. The dashed line corresponds to the classic SPT prediction for the Tolman length, Eq. 10 in (Stillinger, 1973).

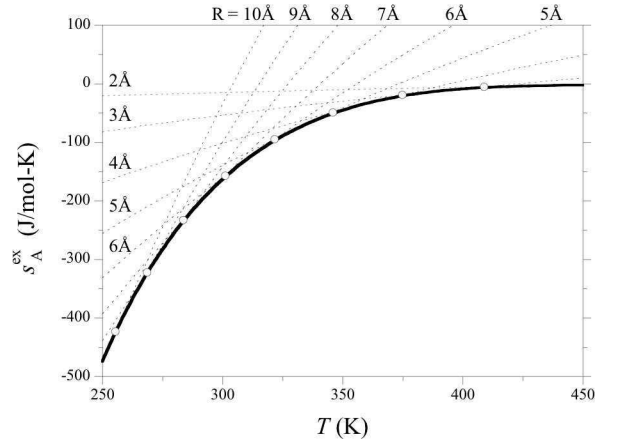


FIG. 13 Entropy of hydrophobic hydration as a function of temperature for solutes in the size range  $2 \text{ \AA} < R < 10 \text{ \AA}$  in  $1 \text{ \AA}$  increments. The dashed lines are the excess entropies of hydration. The open circles are the convergence temperatures for consecutive solutes, *i.e.*,  $s_A^{\text{ex}}(R) = s_A^*(R + 1 \text{ \AA})$ . The thick solid line indicates the entropy convergence temperature in the limit of infinitesimal perturbations in  $R$ .

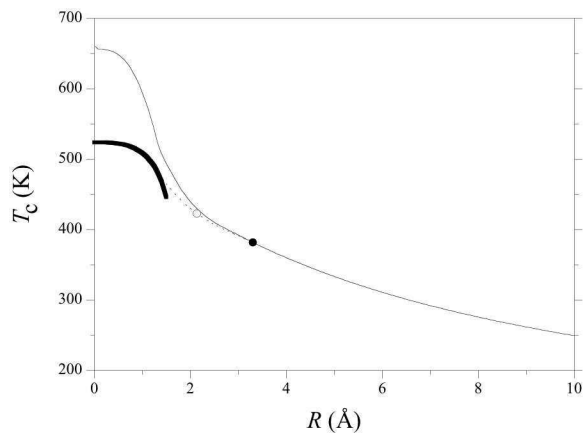


FIG. 14 Variation of the entropy convergence temperature with increasing hard-sphere radius. The thin solid line is the convergence temperature determined under the assumption the heat capacity is independent of temperature. The thick solid line is the exact entropy convergence temperature for  $R < \sigma_{\text{WW}}/2$  from Eq. (22). The dashed line smoothly interpolates between the exact and constant heat capacity curves at 1.25 Å and 3.3 Å, respectively. The filled circle indicates the entropy convergence temperature of a methane-sized solute ( $T_c = 382$  K). The open circle indicates the entropy convergence temperature based on the IT criterion ( $T_c = 420$  K).